Chain length of saturated fatty acids regulates mitochondrial trafficking and function in sensory neurons

Amy E. Rumora,* Giovanni LoGrasso,* Julia A. Haidar,* Justin J. Dolkowski,† Stephen I. Lentz,† and Eva L. Feldman[1,*]

Departments of Neurology* and Internal Medicine,† University of Michigan, Ann Arbor, MI 48109

Abstract **Dyslipidemia associated with T2D leads to diabetic neuropathy, a complication characterized by sensory neuronal dysfunction and peripheral nerve damage. Sensory dorsal root ganglion (DRG) neurons are dependent on axonal mitochondrial energy production facilitated by mitochondrial transport mechanisms that distribute mitochondria throughout the axon. Because long-chain saturated FAs (SFAs) damage DRG neurons and medium-chain SFAs are reported to improve neuronal function, we evaluated the impact of SFA chain length on mitochondrial trafficking, mitochondrial function, and apoptosis. DRG neurons were exposed to SFAs with C12:0−C18:0 chain lengths and evaluated for changes in mitochondrial trafficking, mitochondrial polarization, and apoptosis. DRG neurons treated with C16:0 and C18:0 SFAs showed a significant decrease in the percentage of motile mitochondria and velocity of mitochondrial trafficking, whereas C12:0 and C14:0 SFAs had no impact on motility. Treatment with C16:0 and C18:0 SFAs exhibited mitochondrial depolarization correlating with impaired mitochondrial motility; the C12:0- and C14:0-treated neurons retained mitochondrial polarization. The reduction in mitochondrial trafficking and function in C16:0- and C18:0-treated DRG neurons correlated with apoptosis that was blocked in C12:0 and C14:0 SFA treatments. These results suggest that SFA chain length plays an important role in regulating axonal mitochondrial trafficking and function in DRG neurons.**—Rumora, A. E., G. LoGrasso, J. A. Haidar, J. J. Dolkowski, S. I. Lentz, and E. L. Feldman. **Chain length of saturated fatty acids regulates mitochondrial trafficking and function in sensory neurons. *J. Lipid Res.* 2019.** 60: **58–70.**

Supplementary key words diabetes • dyslipidemias • apoptosis • palmitate • stearate • laurate • myristate • mitochondrial depolarization

Diabetic peripheral neuropathy (DPN) is a common complication that affects up to 30% of patients with prediabetes and 50% of T2D patients (1, 2). Patients with DPN experience a loss of sensation that occurs in a stocking-and-glove distribution and has a severe impact on the individual's quality of life and societal productivity (3–7). The progressive loss of sensory function results from distal-to-proximal peripheral nerve damage and dysfunction of sensory neurons. Although the pathogenesis of DPN is not fully understood, recent studies indicate that DPN pathogenesis is directly linked to a continuum of metabolic factors associated with dyslipidemia (8–10).

Plasma concentrations of free saturated FAs (SFAs) are commonly elevated in T2D (11). In general, SFAs are classified as inducers of lipotoxicity (12, 13), mitochondrial dysfunction (14–17), and apoptosis (17); however, recent evidence indicates that hydrocarbon chain length of SFAs defines the level of intracellular lipotoxicity (18, 19). Moreover, the Western diet, characterized by increased intake of foods with high levels of long-chain SFAs (LCSFAs), including myristate (C14:0), palmitate (C16:0), and stearate (C18:0), and low levels of beneficial medium-chain SFAs (MCSFAs), such as laurate (C12:0) (20–22), is a driving factor in the onset of dyslipidemia and T2D (23). MCSFAs are reported to prevent lipotoxicity and increase mitochondrial energy production (18, 24, 25). Likewise, equimolar caloric intake of MCSFAs and LCSFAs increases mitochondrial energy expenditure and leads to oxidative metabolic pathways as opposed to the metabolic dysfunction triggered by LCSFAs (24, 26). SFAs are also directed to mitochondrial oxidative pathways through hydrocarbon chain length-dependent mechanisms; LCSFAs are targeted into the mitochondrial matrix for β-oxidation through a transport system consisting of palmitoyltransferases (18, 24, 27), whereas MCSFAs are transported independently into the mitochondria, allowing for more efficient modulation of mitochondrial energy production (18, 24). Hence, chain length of SFAs plays a critical role in regulating mitochondrial

This study was supported by National Institutes of Health Grants R24 DK082841 and R01 DK107956 (E.L.F.) and F32 1F32DK112642 and T32 1T32DK101357 (A.E.R.); National Institute of Diabetes and Digestive and Kidney Diseases (NIDDK) DiaComp Award DK076169 (E.L.F); Novo Nordisk Grant NNF14OC0011633 (E.L.F.); the American Diabetes Association; the Program for Neurology Research and Discovery; and the A. Alfred Taubman Medical Research Institute. The content is solely the responsibility of the authors and does not necessarily represent the official views of the National Institutes of Health. The authors declare no conflicts of interest.

Manuscript received 15 May 2018 and in revised form 17 October 2018.

Published, JLR Papers in Press, November 15, 2018
DOI https://doi.org/10.1194/jlr.M086843

Abbreviations: DPN, diabetic peripheral neuropathy; DRG, dorsal root ganglion; LCSFA, long-chain saturated FA; MCSFA, medium-chain saturated FA; RLU, relative light unit; SFA, saturated FA; TM, treatment medium; TMRM, tetramethylrhodamine methyl ester.

[1]To whom correspondence should be addressed.
e-mail: efeldman@umich.edu

function; however, the impact of SFA hydrocarbon chain length on mitochondrial function in sensory neurons is unknown.

Dorsal root ganglion (DRG) sensory neurons require mitochondrial energy production throughout the length of the axon to facilitate neuronal function (28). This requires molecular motors, including kinesin-1 and dynein, to distribute mitochondria throughout the length of the axon in an anterograde and retrograde direction, respectively. Mitochondrial trafficking mechanisms and mitochondrial function are regulated by a complex network of both post-translational cues and the metabolic state to maintain axonal energy homeostasis (29–33). Interestingly, our recent studies indicate that mitochondrial trafficking mechanisms are tightly regulated by the LCSFA palmitate, which impairs mitochondrial transport in DRG neurons and impairs mitochondrial function (16). In this study, we evaluated the metabolic effects of SFA hydrocarbon chain length on mitochondrial axonal transport, mitochondrial function, and apoptosis in DRG sensory neurons.

MATERIALS AND METHODS

Primary DRG neuron cultures

DRG neuron preparation for confocal imaging included dissection of adult C57Bl/6J mice, dissociation of extracted DRGs, and culture of DRG neurons per our previously published protocols (16, 34–36). All animal work protocols adhered to the state, federal, and University of Michigan guidelines accredited by the Association for the Assessment and Accreditation of Laboratory Animal Care International. Protocols were approved by the University of Michigan Institutional Animal Care and Use Committee (Protocol no. PRO00008115). Briefly, cervical, lumbar, and thoracic DRGs were extracted from 16−18 wk old C57Bl/6J mice (The Jackson Laboratory, Bar Harbor, ME) and collected in L15 medium (Lonza, Basel, Switzerland). Subsequent to a 30 min incubation in 2 mg/ml collagenase (Millipore-Sigma, Billerica, MA), DRGs were dissociated into a single-cell suspension by consecutive trituration with a Pasteur pipet and a fire-polished glass pipet in heat-inactivated BSA. Dissociated neurons were resuspended in primary DRG neuron treatment medium (TM) [50% F-12K (Cell Gro; Corning, Manassas, VA) and 50% DMEM (Cell Gro; Corning), 1:100 dilution of Nb^{+}, 1,000 U/ml penicillin/streptomycin/neomycin (Thermo Fisher Scientific, Waltham, MA), and 7.2 μM aphidicolin (Millipore-Sigma)] supplemented with 1× B27 and 0.4 μM L-glutamine (16). Neurons were transfected with 3.75 μl/ml CellLight mitochondria-GFP (mito-GFP BacMam 2.0, Thermo Fisher Scientific) prior to plating on 4-well 25 μg/ml laminin-coated (Millipore-Sigma) Nuc Lab-Tek chambered coverglass imaging plates (Thermo Fisher Scientific). DRG neurons adhered after 24 h, and medium was replaced with primary DRG neuron feed medium (TM containing 1× B27) (16) for another 24 h. Within 48 h after plating, DRG neurons extended axons and were treated with SFAs ranging in hydrocarbon chain lengths from C12:0−C18:0.

SFA treatments

DRG neuron cultures were treated for 24 h with 31.25−250 μM laurate (C12:0), myristate (C14:0), palmitate (C16:0), or stearate (C18:0). All SFAs were conjugated to FA-free BSA (Thermo Fisher Scientific) as described previously (16) and diluted to final concentration(s) in TM. A TM control was used to establish the basal level of mitochondrial trafficking in DRG neurons. A 0.25% BSA vehicle control was used to evaluate the effect of BSA alone (0.25% BSA was present in the highest 250 μM SFA treatment groups). To evaluate whether mitochondrial trafficking could be restored after SFA treatments, DRG neuron cultures were treated with 62.5, 125, or 250 μM palmitate or stearate for 12 h, washed twice with TM, and replaced with TM for 12 h. A 12 h treatment with 62.5, 125, or 250 μM palmitate or stearate was a negative control to establish the level of impaired mitochondrial trafficking after 12 h of SFA treatment.

Mitochondrial trafficking and kymograph analysis

Mitochondrial axonal transport was visualized by confocal time-lapse microscopy as previously described (16, 37). Briefly, mitochondrial movement in DRG axons was imaged on a Nikon A1 confocal microscope (Nikon Instruments, Melville, NY) equipped with NIS Elements software (Nikon Instruments) and a Tokai Hit environmental chamber (Tokai Hit, Shizuoka-ken, Japan) to maintain DRG neurons at 5% CO_2 and 37°C. Microscope settings were optimized for recording axonal mitochondrial movement using a 40× oil objective with a confocal aperture set at a 4.49 μm optical thickness. For each DRG neuron, mitochondrial motility was recorded by taking a 2× zoom image every 2.5 s for 2.5 min using the NIS Elements ND acquisition.

Image analysis was completed using a kymograph analysis with MetaMorph Software (Molecular Devices, Sunnyvale, CA) as described previously (16). For each neuron, an anterograde region of interest was drawn along the axon and used to record mitochondrial movement within 10 μm of the region of interest, generating two kymographs to highlight motile mitochondria and stationary mitochondria (16, 37–39). These kymographs were used to assess the average percentage of motile mitochondria, mitochondrial bidirectionality (either anterograde or retrograde), and mitochondrial velocity. Mitochondria with a velocity less than a threshold velocity of 0.02 μm/s were considered stationary (16, 37). Mitochondrial trafficking results were derived from an average of 17 neurons for each SFA treatment from three separate experimental replicates.

Mitochondrial depolarization analysis

To assess the effect of SFA hydrocarbon chain length on mitochondrial depolarization, DRG neurons were labeled with a mitochondrial membrane potential-dependent fluorophore, tetramethylrhodamine methyl ester (TMRM) (Thermo Fisher Scientific) (36, 40, 41), as described previously (16). Primary DRG neurons were transfected with mito-GFP, cultured for 48 h, and treated with 125 μM laurate, myristate, palmitate, and stearate as described above. After 24 h of treatment, DRG neurons were stained with 50 nM TMRM for 30 min at 37°C. Single sequential images of DRG neurons were taken in both the red channel (TMRM signal) and green channel (mito-GFP signal) on a Nikon A1 confocal microscope. Images of TMRM staining intensity were analyzed by masking the TMRM signal to mito-GFP labeled mitochondria using the MetaMorph Image Analysis program (Molecular Devices). A threshold TMRM intensity was set at 1,000 intensity units (1.5% max, range 0–65,536), and all mitochondria with TMRM staining below 1,000 were marked as depolarized. An average of 36 neurons were evaluated from three experimental replicates for each treatment condition.

50B11 DRG neuron cell culture and differentiation

To evaluate the dependence of ATP production and apoptotic activation on SFA hydrocarbon chain length in DRG neurons, an

immortalized 50B11 DRG neuron cell line (42) was treated with physiological concentrations of laurate, myristate, palmitate, or stearate. Briefly, 50B11 cells were cultured in 50B11 Neurobasal medium (Gibco) containing 10% (v/v) heat-inactivated FBS (Gibco), 0.2% (v/v) glucose, 0.5 mM L-glutamine (Gibco), and 5.6× B27 (Gibco). The 50B11 cells were plated in triplicate in a 96-well assay plate at 10,000 cells/well. Cells were grown for 48 h and then differentiated on the assay plate by exchanging the plating medium for 50B11 Neurobasal medium containing 75 μM forskolin (Sigma). After 12 h of exposure to forskolin, 50B11 neurons extended axons and were treated with physiological concentrations of 62.5−250 μM MCSFAs and LCSFAs for 24 h. SFA treatments were prepared as described above in 50B11 Neurobasal medium containing 75 μM forskolin.

Caspase-Glo 3/7 and CellTiter-Glo assays

SFA-treated differentiated 50B11 DRG neurons were evaluated for ATP level using a CellTiter-Glo kit (Promega, Madison, WI) or for apoptosis using a Caspase-Glo 3/7 assay Kit (Promega) after 24 h of SFA treatment, according to the manufacturer's protocol. To assess ATP production in SFA-treated 50B11 cells, a 1:1 ratio of CellTiter-Glo reagent was added to each well. Apoptotic activity was evaluated by mixing Caspase-Glo 3/7 reagent with 50B11 cell culture medium at a 1:1 ratio. The luminometric reactions were mixed on a rotating shaker for 30 s and incubated at room temperature for 1 h. Luminometric signals from each well were read at 30 min and 1 h time points on a Synergy|HTX multimode plate reader (BioTek, Winooski, VT) equipped with Gen5 software (version 3.03) using integration times of 500 and 1,000 ms. An average of 6 wells of 50B11 DRG neurons from each SFA treatment condition were analyzed from two experimental replicates.

Mitochondrial morphology analysis

Images from mitochondrial trafficking studies were processed through an ImageJ macro to evaluate alterations in mitochondrial circularity and mitochondrial size. Images were analyzed from each 250 μM SFA treatment condition and the corresponding 0.25% vehicle control at a 1,024 × 1,024 resolution using the NIS-Elements Software (Nikon Instruments). Mitochondrial morphology analysis was performed using a mitochondrial morphology macro in Fiji to determine mitochondrial circularity and area as described previously (43, 44). To determine mitochondrial size distribution, the mitochondria were binned into different size categories with each bin increasing by 2 μm^2 (45) using a frequency distribution and Kolmogorov-Smirnov test to show SFA-induced statistically significant changes in mitochondrial size (46).

Statistics

Statistical analyses of all studies were completed using Prism, Version 7 (GraphPad Software, La Jolla, CA). Results from mitochondrial trafficking studies, mitochondrial depolarization studies, and Caspase-Glo 3/7 assays are expressed as means ± SEM. Data resulting from mitochondrial trafficking, mitochondrial depolarization, CellTiter-Glo, and Caspase-Glo 3/7 studies were analyzed for significance using one-way ANOVA and Tukey's posthoc test for multiple comparisons. Mitochondrial circularity results were analyzed for statistical significance with an unpaired *t*-test and mitochondrial size was evaluated using the Kolmogorov-Smirnov test (46). Mitochondrial trafficking and mitochondrial depolarization studies exhibited statistical significance at $P < 0.01$, CellTiter-Glo assays were significant at $P < 0.0001$, and mitochondrial morphology studies and Caspase-Glo 3/7 experiments showed statistical significance at $P \leq 0.05$.

RESULTS

LCSFAs reduce the percentage of motile mitochondria

To assess the dependence of axonal mitochondrial trafficking on SFA hydrocarbon chain length, DRG neurons were treated with physiologic concentrations of MCSFAs and LCSFAs, and mitochondrial movement was evaluated by time-lapse confocal microscopy and kymograph analyses (**Fig. 1A**). Approximately 40% of the axonal mitochondria were motile in DRG neurons exposed to TM and 0.25% BSA controls without SFA treatments. The percentage of motile mitochondria was not significantly impacted in DRG neurons treated with laurate (C12:0) (Fig. 1A, B) or myristate (C14:0) (Fig. 1A, C) at concentrations ranging from 31.25 to 250 μM. Conversely, treatment with concentrations ranging from 62.5 to 250 μM palmitate (Fig. 1A, D) and 31.25 to 250 μM stearate (Fig. 1A, E) resulted in a dose-dependent reduction in mitochondrial motility. Stearate and palmitate at a concentration of 250 μM reduced the percentage of motile mitochondria from approximately 40% to 5–10%, whereas 250 μM laurate and myristate retained 30–40% of motile mitochondria. The 62.5–250 μM palmitate and stearate 12 h treatments significantly impaired mitochondrial transport, similar to the 24 h treatments. However, washout experiments showed that axonal mitochondrial transport was only partially restored 12 h after the palmitate (Fig. 1F) or stearate (Fig. 1G) treatments had been replaced with TM, but these changes were not significant. Hence, DRG neurons treated with physiologic concentrations of the LCSFAs palmitate (C16:0) and stearate (C18:0) exhibited impaired mitochondrial motility, whereas treatment with the shorter-chain SFAs laurate (C12:0) and myristate (C14:0) had no effect.

Mitochondrial trafficking directionality is mildly affected by LCSFAs

Bidirectional mitochondrial transport is essential for maintaining a functional population of axonal mitochondria at distal regions of DRG axons for ATP production (16, 17, 28). Therefore, we investigated whether SFAs offset the balance between anterograde transport of healthy mitochondria away from the cell body into the axon and retrograde clearance of old mitochondria from the axon back toward the cell body. The percentage of motile mitochondria trafficking in the anterograde and retrograde direction was not significantly altered by laurate (C12:0) (**Fig. 2A**) or myristate (C14:0) (Fig. 2B). DRG neurons treated with 250 μM palmitate exhibited a reduction in anterograde mitochondrial transport; however, these results are not significant because the directionality of mitochondrial movement was only evaluated in 8% of motile mitochondria after 24 h of 250 μM palmitate treatment (Fig. 2C; see also Fig. 1D). Stearate, conversely, exhibited a trending dose-dependent increase in the percentage of anterograde moving mitochondria at concentrations of 62.5–250 μM (Fig. 2D). Taken together, these data indicate that only trending alterations in the bidirectionality of mitochondrial movement occur in the presence of higher physiologic concentrations of the LCSFAs palmitate and stearate.

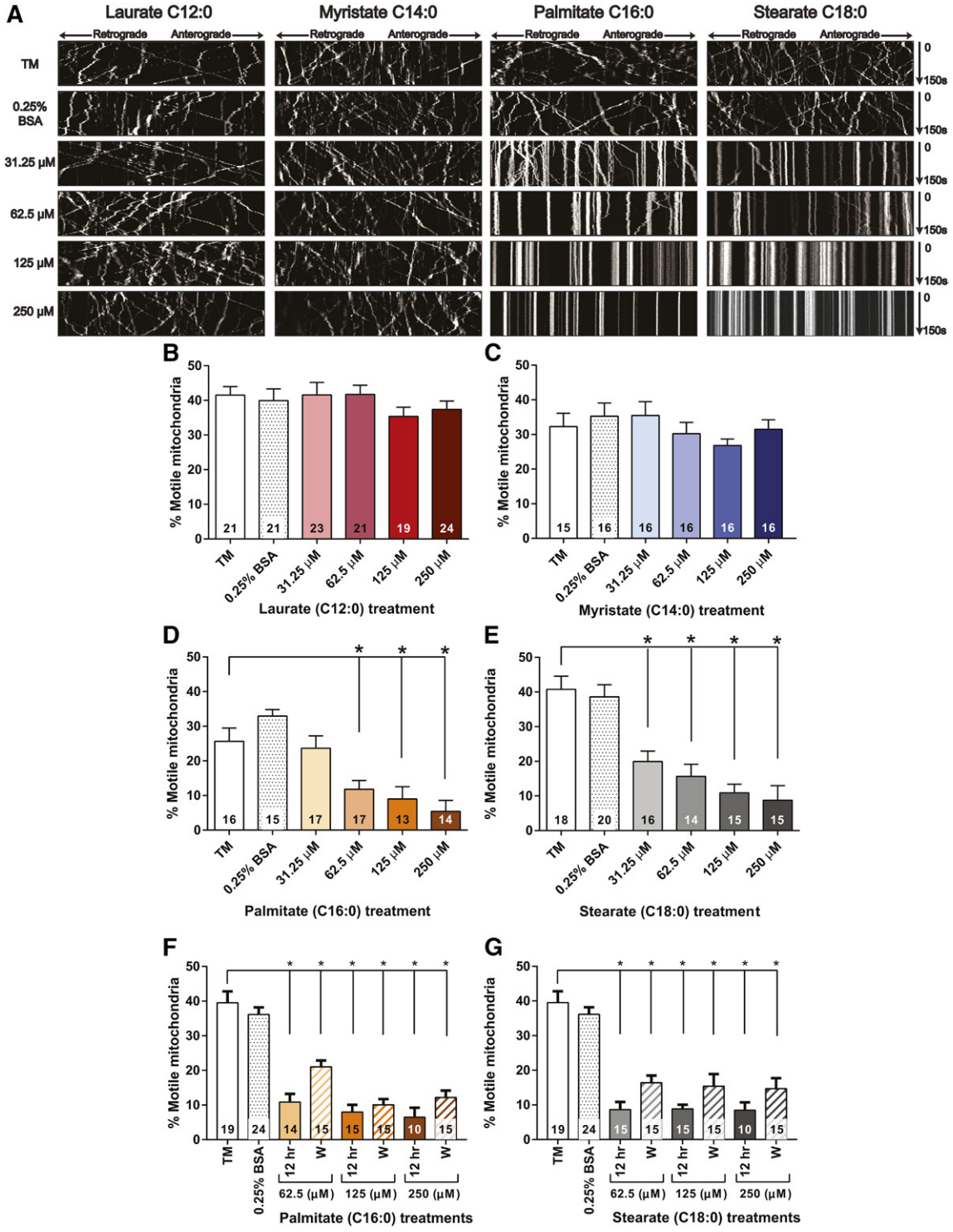

Fig. 1. LCSFAs palmitate and stearate induce a dose-dependent decrease in mitochondrial trafficking in mouse DRG neurons. A: Representative kymographs from each treatment condition show the movement of individual mitochondria (white lines) from 0 to 150 s. Anterograde moving mitochondria (→) are identified as lines moving toward the right of the kymograph, and retrograde mitochondria (←) migrate toward the left of the kymograph as the time progresses from 0 to 150 s. A distinct decrease in the number of motile mitochondria was observed in DRG neurons treated with increasing concentrations of palmitate and stearate compared with laurate and myristate. B, C: Laurate and myristate had no significant impact on the percent motile mitochondria. D: Palmitate induced a dose-dependent decrease in the percent motile mitochondria at concentrations ranging from 62.5 to 250 µM. E: Stearate induced a dose-dependent reduction in mitochondrial trafficking from 31.25 to 250 µM. F, G: Mitochondrial transport was partially recovered in DRG neurons exposed to a 12 h TM wash (W) after a 12 h palmitate (F) or stearate (G) treatment at all concentrations ranging from 62.5 to 250 µM. The percentage of motile mitochondria was slightly increased compared with the 12 h palmitate (F) or stearate treatments (G), but the increase in axonal mitochondrial trafficking was not significant. The number within each bar represents the total number of DRG neurons that were evaluated for each treatment condition across three separate experimental trials. Values are expressed as mean ± SEM. * $P < 0.01$, ordinary one-way ANOVA with Tukey's multiple-comparisons test.

Velocity of mitochondrial motility is reduced by LCSFA treatment

Because stationary mitochondria in DRG axons have the capacity to slow organellar transport in the anterograde and retrograde directions in healthy DRG neuronal cultures (47, 48), and because the slowing of organellar transport was observed in healthy DRG neurons in culture (47), we next sought to determine whether an increase in the number of stationary mitochondria in LCSFA-treated DRG neurons led to an overall reduction in mitochondrial velocity (**Figs. 3**, **4**). Mitochondrial trafficking in DRG neurons treated with laurate (Figs. 3A, 4A) and myristate (Figs. 3B, 4B) retained anterograde and retrograde velocities ranging from 0.15 to 0.25 μm/s, similar to those of the TM and 0.25% BSA controls. Conversely, treatment with palmitate induced a trending dose-dependent decrease in anterograde (Fig. 3C) and retrograde (Fig. 4C) velocities of motile mitochondria, whereas treatment of DRG neurons with 31.25–250 μM stearate induced significant dose-dependent reductions in both anterograde (Fig. 3D) and retrograde (Fig. 4D) mitochondrial velocities. These data indicate that C16:0–C18:0 LCSFA-treated DRG neurons exhibit a dose-dependent reduction in mitochondrial velocity, whereas treatment with shorter-chain SFAs have no effect, further suggesting that the number of stationary mitochondria may have a direct impact on mitochondrial trafficking velocity.

LCSFAs induce mitochondrial depolarization

Impairment of mitochondrial trafficking correlates with a reduction in mitochondrial membrane potential in palmitate-treated DRG neurons (16, 36, 49); therefore, we next assessed the effect of SFA hydrocarbon chain length on mitochondrial depolarization. We measured mitochondrial depolarization using a cationic red fluorescent probe, TMRM, that accumulates in the mitochondrial matrix of functional mitochondria but diffuses during a loss of mitochondrial membrane potential (**Fig. 5A**). Bright TMRM staining indicative of polarized mitochondria in the TM and 0.25% BSA control established a baseline of ∼10% of mitochondria that were depolarized (Fig. 5A, B). Treatment with both laurate and myristate retained mitochondrial membrane potential, with no significant increase in the percentage of depolarized mitochondria, whereas treatment with palmitate and stearate both induced a hydrocarbon chain length-dependent increase in mitochondrial depolarization (Fig. 5B). Mitochondrial depolarization resulting from palmitate and stearate treatments correlated with a significant reduction in ATP production in 50B11 DRG neurons (Fig. 5C). Both 125–250 μM palmitate and 125–250 μM stearate treatments resulted in a dose-dependent reduction in ATP, whereas laurate and myristate had no impact on ATP level. The 250 μM stearate treatment nearly abolished ATP production, reducing the ATP level by over 92%. This impairment in mitochondrial function is also associated with alterations in mitochondrial morphology, evidenced by an increase in mitochondrial size and circularity in DRG neurons treated with 250 μM stearate and 250 μM palmitate (**Fig. 6C**, D, G, H). These alterations in mitochondrial morphology did not occur in DRG neurons treated with 250 μM laurate (Fig. 6A, E) and 250 μM myristate (Fig. 6B, F). Together, these data indicate that mitochondrial membrane potential, mitochondrial function, and mitochondrial morphology are dependent on SFA hydrocarbon chain length.

LCSFAs induce apoptosis

Because SFA treatment can mediate apoptosis (50, 51), the level of apoptosis was examined in 50B11 DRG neurons treated with elevated concentrations of SFAs. Caspase 3/7 activity level, measured by the mean normalized relative light units (RLUs), was 0.1 RLU for DRG neurons from the TM and 0.25% BSA control groups (**Fig. 7**). Similarly, neurons treated with 62.5–250 μM laurate or myristate did not exhibit significant increases in caspase 3/7 activity (Fig. 7). Conversely, 50B11 DRG neurons treated with 125–250 μM palmitate or stearate exhibited significant dose-dependent increases in caspase 3/7 activity, with RLUs approximately 8–10 times higher than those of the controls. Interestingly, 62.5 μM palmitate or stearate did not lead to increases in caspase 3/7 activity, despite the fact that this treatment significantly impaired mitochondrial trafficking (Figs. 1D, E, 2C, D, 3C, D, and 4C, D).

DISCUSSION

We examined the impact of SFA hydrocarbon chain length on mitochondrial trafficking, mitochondrial dysfunction, and apoptosis in sensory DRG neurons based on previous studies suggesting that nerve damage and sensory neuronal dysfunction underlying the progression of DPN is linked to an increased intake of SFAs associated with the Western diet (9, 10, 17). We found that 24 h treatments with LCSFAs at physiological concentrations of 62.5–250 μM palmitate and 31.25–250 μM stearate significantly impaired mitochondrial axonal trafficking in a dose-dependent manner, whereas treatments with 31.25–250 μM MCSFA laurate and 31.25–250 μM LCSFA myristate had no significant impact on mitochondrial movement in DRG axons after 24 h. Moreover, the impairment of mitochondrial trafficking by palmitate and stearate correlated with a reduction in mitochondrial membrane potential and ATP, altered mitochondrial morphology, and an induction of neuronal apoptosis that was not observed in DRG neurons treated with laurate or myristate. Collectively, these data suggest that increases in the LCSFAs palmitate and stearate impair mitochondrial trafficking and mitochondrial function and induce the initiation of DRG neuronal apoptosis.

The Western diet is enriched in SFAs that are linked to the development of neurodegenerative diseases (52–54). Recent studies indicate that the FA composition and the source of fat in high-fat-diet mouse models significantly contributes to downstream molecular dysfunction (55). Lard-based high-fat diets that are used to mimic the Western diet consist of greater LCSFAs and few MCSFAs (56, 57). Interestingly, C57Bl/6J mice fed lard-based high-fat diets develop peripheral neuropathy and the metabolic

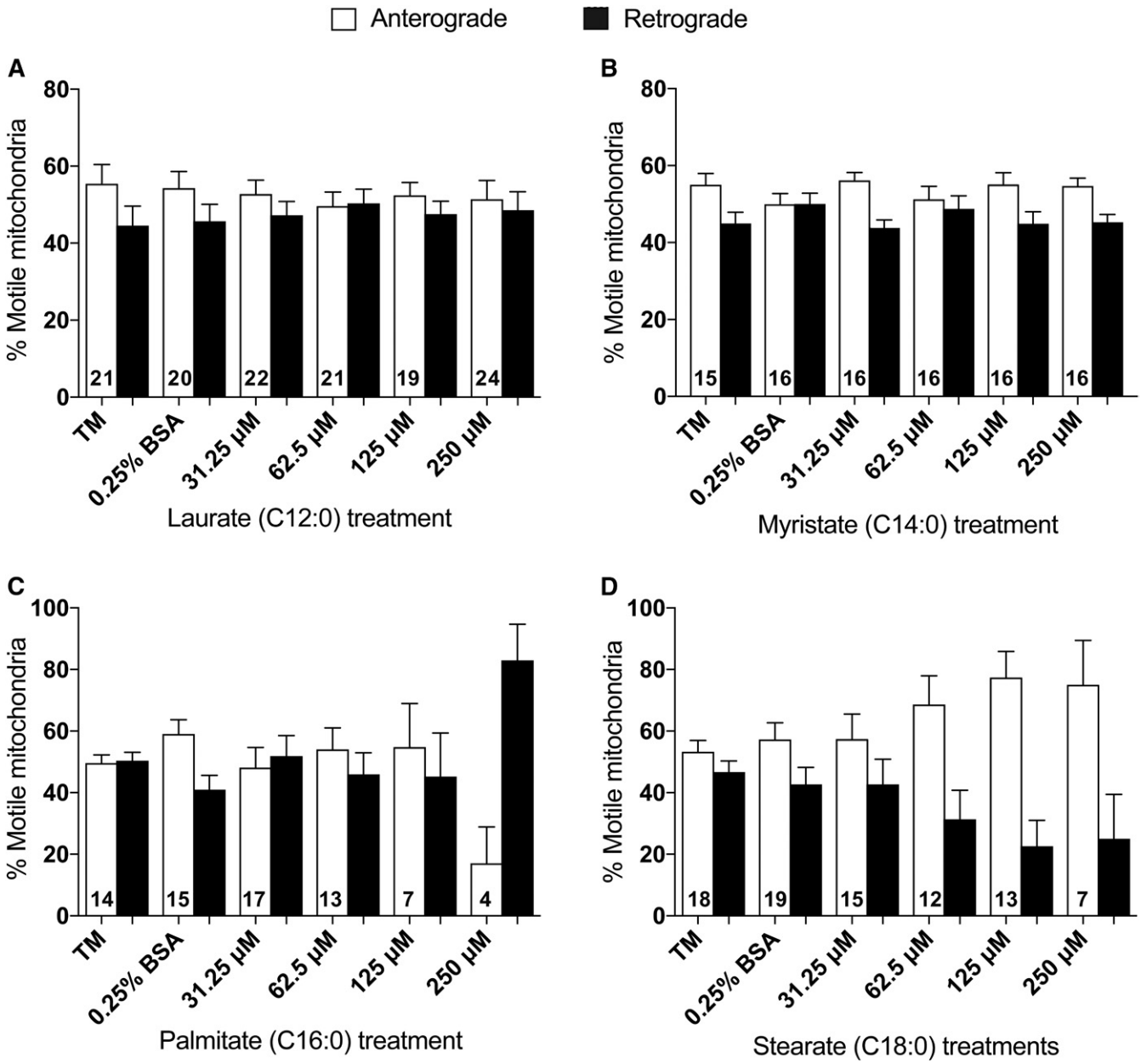

Fig. 2. LCSFA stearate treatment exhibits a preference for anterograde mitochondrial trafficking. A, B: Laurate and myristate showed no significant alteration in directionality of mitochondrial trafficking after 24 h treatments. C: Similarly, DRG neurons treated with palmitate for 24 h did not exhibit a preference for anterograde (open bars) or retrograde (filled bars) directionality, although a visible but nonsignificant reduction in anterograde mitochondrial transport was noted at 250 µM palmitate. D: Treatments of 125–250 µM stearate induced a trending, dose-dependent increase in anterograde mitochondrial trafficking relative to retrograde mitochondrial directionality. The total number of DRG neurons that were evaluated for anterograde and retrograde mitochondrial directionality in each treatment condition are given in each set of bars. Values are expressed as mean ± SEM.

defects associated with T2D, including weight gain, hyperinsulinemia, impaired glucose tolerance, increased HbA1c, and dyslipidemia (10, 58). Modeling dyslipidemia in cultures of sensory DRG neurons also induces significant neuronal damage, including oxidative stress, impaired mitochondrial trafficking, dysfunctional axonal mitochondria, bioenergetic reprogramming, and neuronal dysfunction as a result of increased levels of LCSFAs (14–17, 27, 59, 60). In parallel, several recent studies also indicate that normalization of MCSFA levels in lard-based high-fat-diet mouse models leads to a reduction in adiposity and insulin resistance associated with T2D (24, 25, 56, 61–63), suggesting that cellular dysfunction is dependent on hydrocarbon chain length. These data support the rationale for our current evaluation of the impact of SFA hydrocarbon chain length on mitochondrial transport and function in the primary sensory DRG neurons damaged in DPN.

The DRG sensory neurons extend axons up to 1 m in length and are dependent on transport mechanisms that shuttle mitochondria throughout the length of the axon to provide energy for neuronal function (28, 29, 64–66). We recently found that DRG neuron mitochondrial trafficking

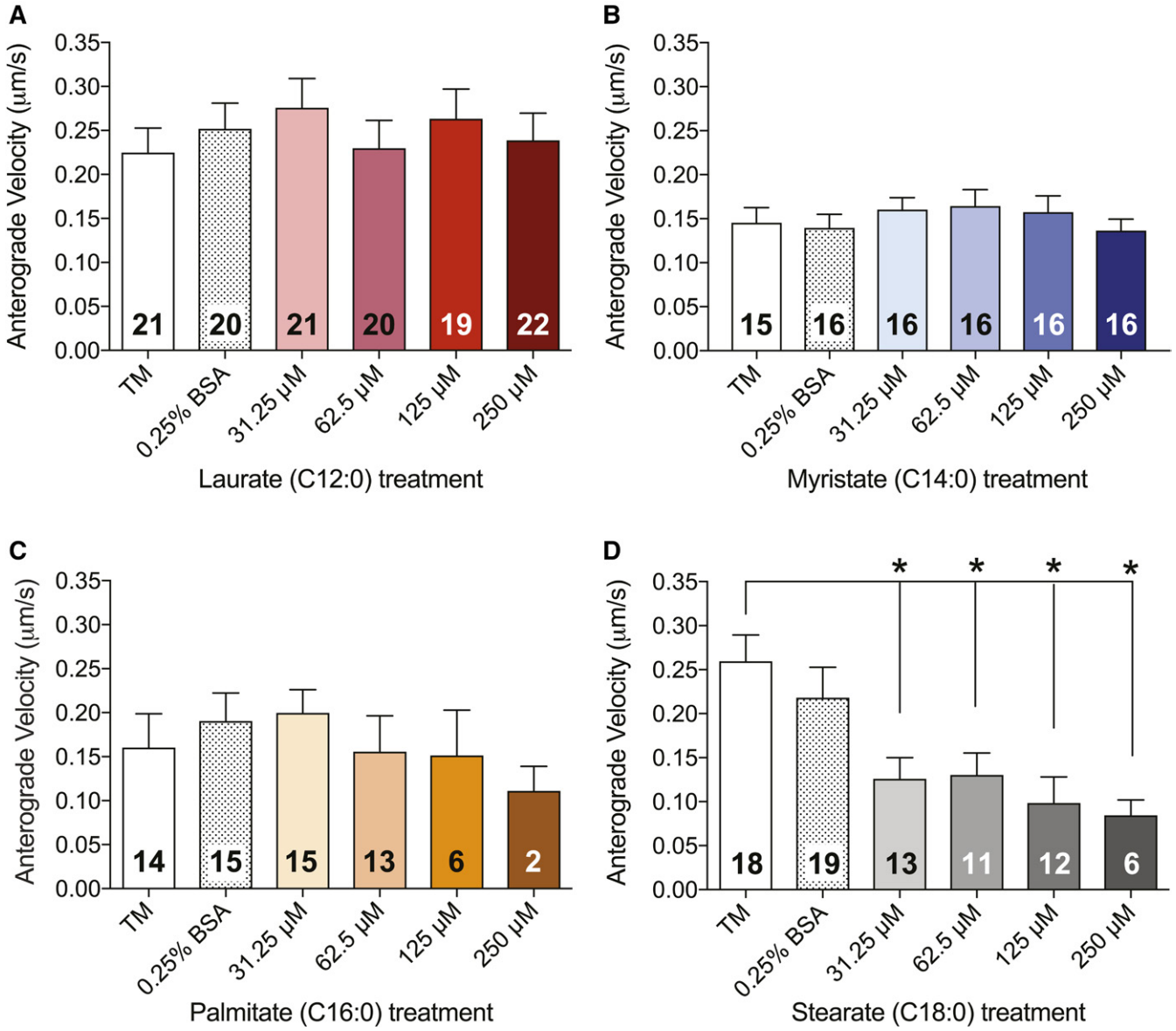

Fig. 3. LCSFAs palmitate and stearate induce dose-dependent reductions in anterograde mitochondrial trafficking velocity in mouse DRG neurons. A, B: Laurate and myristate have no effect on anterograde mitochondrial velocity. Palmitate treatments exhibit a trending dose-dependent decrease in anterograde velocity (C), whereas stearate treatments ranging from 31.25 to 250 μM induce significant dose-dependent reductions in anterograde mitochondrial trafficking velocity after 24 h (D). The number in each bar is the total number of DRG neurons that were evaluated for each treatment condition in three separate experimental trials. Values are expressed as mean ± SEM. * $P < 0.01$, ordinary one-way ANOVA with Tukey's multiple-comparisons test.

mechanisms are unaffected by elevated glucose levels, whereas axonal mitochondrial transport and function are significantly impaired in the presence of the LCSFA palmitate (16). To determine whether MCSFAs and LCSFAs have different effects on DRG neurons, we first assessed the impact of SFA hydrocarbon chain length on the percentage of motile mitochondria in DRG axons. Physiological concentrations of palmitate (C16:0) and stearate (C18:0) significantly reduced mitochondrial trafficking in a dose-dependent manner, whereas laurate (C12:0) and myristate (C14:0) had no effect on the percentage of motile mitochondria. Mitochondrial trafficking was only partially restored 12 h after removal of the LCSFAs palmitate and stearate in washout experiments, showing that LCSFAs induce lasting metabolic dysfunction leading to alterations in mitochondrial trafficking that cannot be repaired by short-term removal of LCSFAs. These results suggest that mitochondrial trafficking is only impaired by treatments with energetically challenging LCSFAs ranging from C16:0 to C18:0, whereas SFAs with shorter hydrocarbon chains (C12:0–C14:0) have no impact on mitochondrial motility. These effects are likely due to the unique metabolic availability of laurate (C12:0) and myristate (C14:0), as they are directed through oxidative pathways and promote higher energy expenditure compared with the LCSFAs palmitate and stearate (26). Passive diffusion of shorter hydrocarbon-chain SFAs into DRG neurons allows for translocation directly into mitochondria for β-oxidation independent of transporter proteins (26, 56). Conversely, translocation of energetically challenging LCSFAs into the DRG neuronal

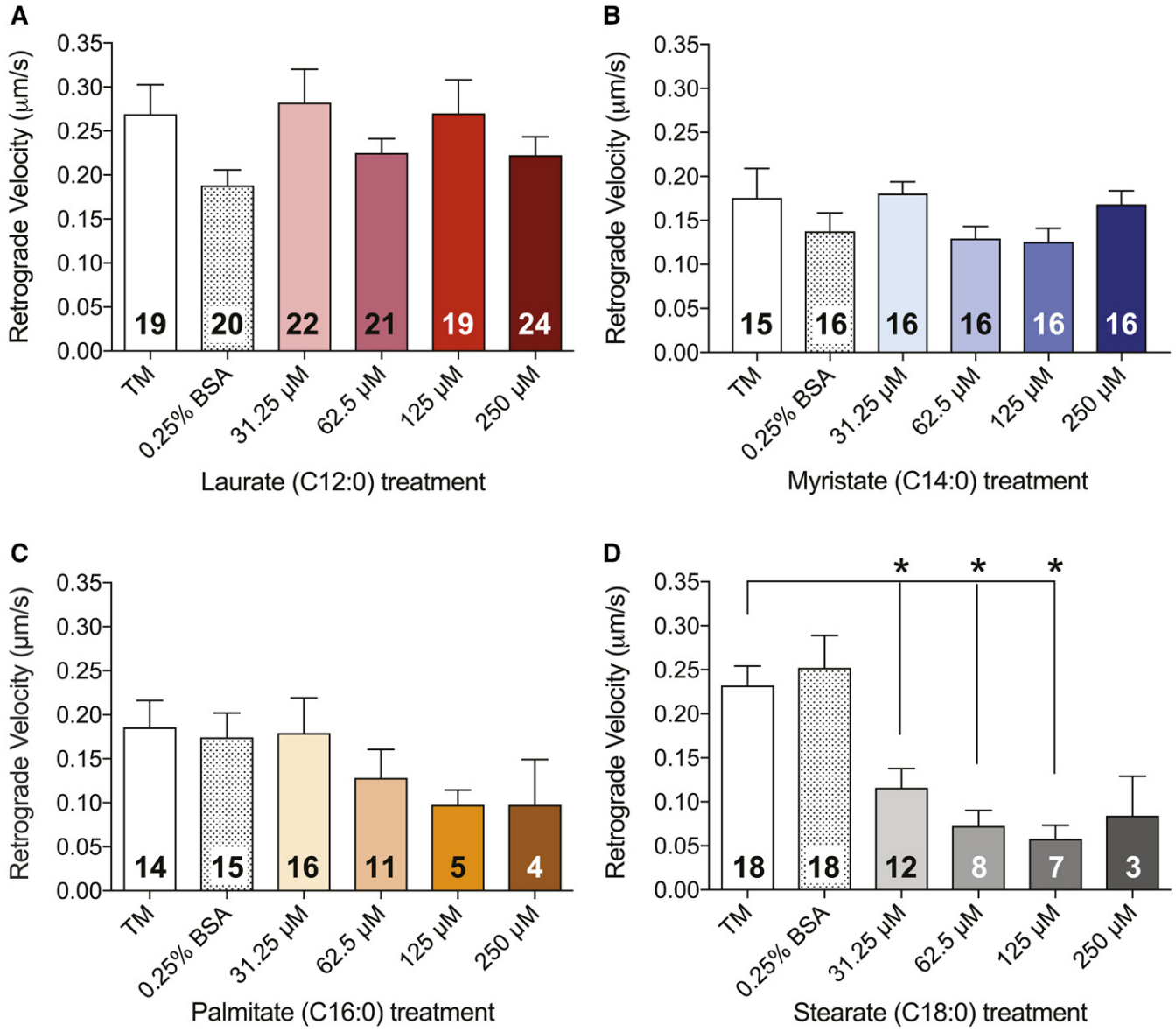

Fig. 4. LCSFAs palmitate and stearate induce dose-dependent reductions in retrograde mitochondrial trafficking velocity in mouse DRG neurons. A, B: Retrograde mitochondrial velocity is unaffected by laurate and myristate treatments. Palmitate treatments ranging from 62.5 to 250 μM induce a trending decrease in retrograde velocity (C), whereas stearate treatments ranging from 31.25 to 125 μM induce a significant dose-dependent decrease in retrograde velocity (D). Each bar contains the total number of DRG neurons analyzed for each treatment condition. Values are expressed as mean ± SEM. * $P < 0.01$, ordinary one-way ANOVA with Tukey's multiple-comparisons test.

mitochondria for β-oxidation requires specialized FA binding proteins and carnitine palmitoyltransferase transporter proteins (19). Excess intracellular levels of LCSFAs palmitate and stearate stimulate the production of lipotoxic lipid intermediates that induce mitochondrial dysfunction, mitochondrial depolarization (67), and bioenergetic reprogramming (15, 16). Therefore, maintenance of mitochondrial transport in laurate- and myristate-treated DRG axons is likely due to the metabolic availability of these SFAs that prevent intracellular stress pathways induced by the LCSFAs palmitate and stearate.

Bidirectional mitochondrial trafficking in DRG axons is essential for the distribution of healthy mitochondria throughout the axon by anterograde mitochondrial transport and the return of unhealthy mitochondria to the cell body for degradation via retrograde transport (28, 31, 68). We found that bidirectional mitochondrial movement was not significantly altered by the MCSFA or LCSFAs evaluated; however, the trending dose-dependent increase in anterograde transport at high concentrations of stearate indicates that a decrease in overall mitochondrial motility may trigger recruitment of the remaining motile mitochondria to the axon to preserve DRG neuronal function. Increased anterograde transport of mitochondria into the axon may be the result of impaired mitochondrial bioenergetics due to lipid overload (15, 16) or lipid-induced molecular changes to the axonal microtubule or mitochondrial transport proteins (66, 69, 70). It is important to note, however, that the average percentage of anterograde or retrograde mitochondrial motility in LCSFA-treated DRG

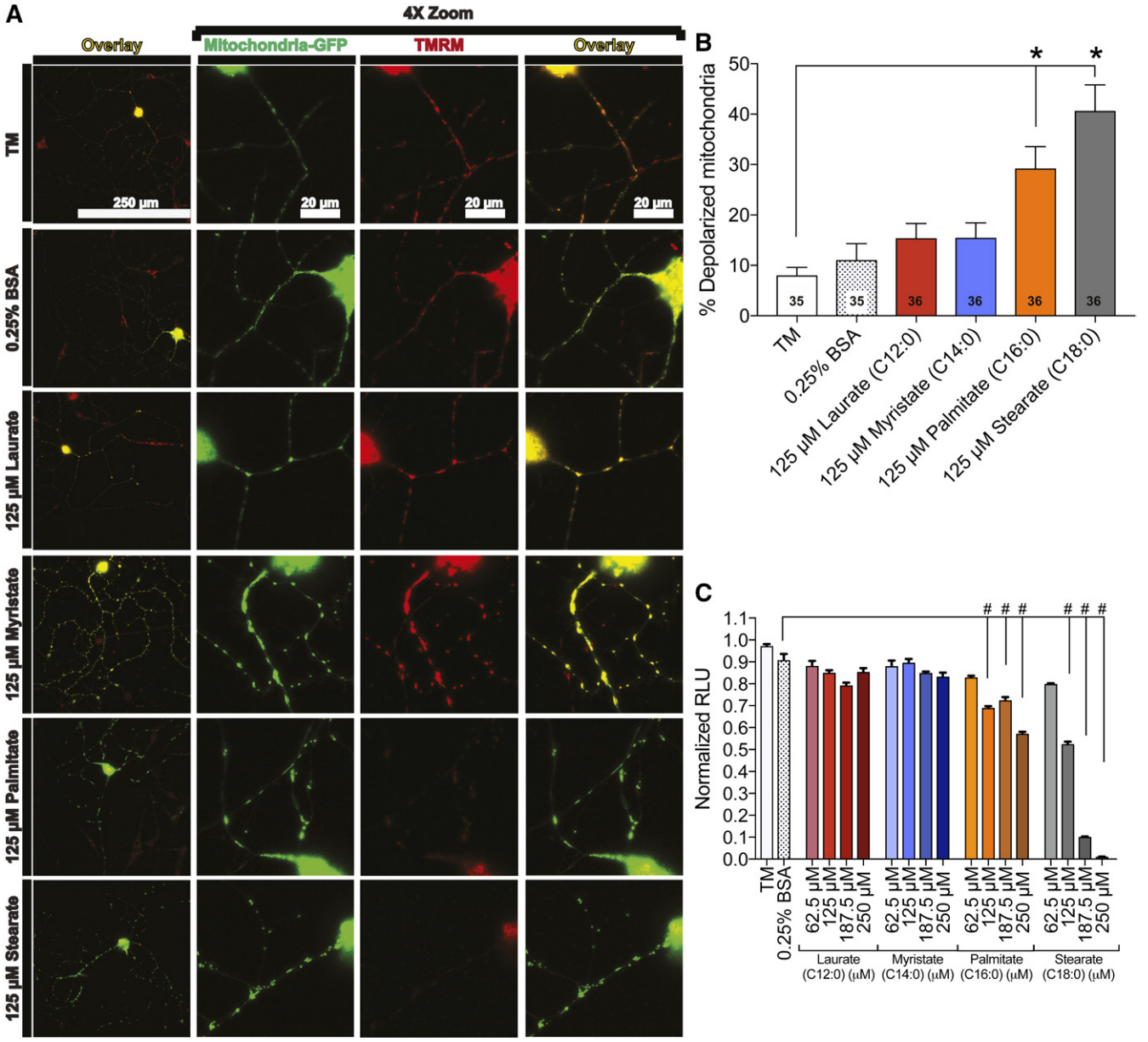

Fig. 5. LCSFAs palmitate and stearate induce mitochondrial depolarization in mouse DRG neurons. A: DRG neurons expressing mito-GFP (green) were evaluated for changes in TMRM staining (red) using an overlay (yellow) of mito-GFP and TMRM signal that appears yellow in polarized mitochondria (left overlay column). Each neuron is displayed with a 4× zoom to depict the mitochondria-GFP signal, TMRM signal, and the merged image (right overlay column). Treatment conditions that retained DRG neuron mitochondrial membrane potential include TM, 0.25% BSA, 125 µM laurate, and 125 µM myristate. The 125 µM palmitate and stearate treatments exhibit diffuse TMRM staining (bottom two rows). B: Quantitation of TMRM signal in DRG neurons treated with 125 µM laurate (red bar) and myristate (blue bar) showed no significant effect on mitochondrial membrane potential relative to the TM and 0.25% BSA controls. Palmitate (orange bar) and stearate (black bar) at a concentration of 125 µM, however, exhibited a significant increase in the percentage of depolarized mitochondria relative to 125 µM laurate, 125 µM myristate, and the TM and 0.25% BSA control-treated neurons. The number displayed in the bar is the total number of DRG neurons that were evaluated for each treatment condition in three separate experimental trials. C: Palmitate- and stearate-treated 50B11 DRG neurons (from 125 to 250 µM) exhibit a reduction in intracellular ATP level compared with the 0.25% BSA control. Laurate and myristate treatments had no effect on ATP level. Values are expressed as mean ± SEM. * $P < 0.01$, ordinary one-way ANOVA with Tukey's multiple-comparisons test (B); $^{\#}P < 0.0001$, ordinary one-way ANOVA with Tukey's multiple-comparisons test (C).

neurons is determined from low numbers of motile mitochondria at high concentrations of stearate and will need to be confirmed in future studies.

The reduction in mitochondrial motility in palmitate- and stearate-treated DRG neurons further correlated with a decrease in mitochondrial trafficking velocity in both the anterograde and retrograde directions; shorter-chain SFAs had no impact on the velocity of mitochondrial axonal movement. These results extend our previous work on palmitate-induced impairment of mitochondrial trafficking velocity (16) and are also in agreement with a recent report indicating that cargo transported along the microtubule in DRG axons reduces velocity in response to stationary axonal cargos (47, 48). These transient pauses occur when

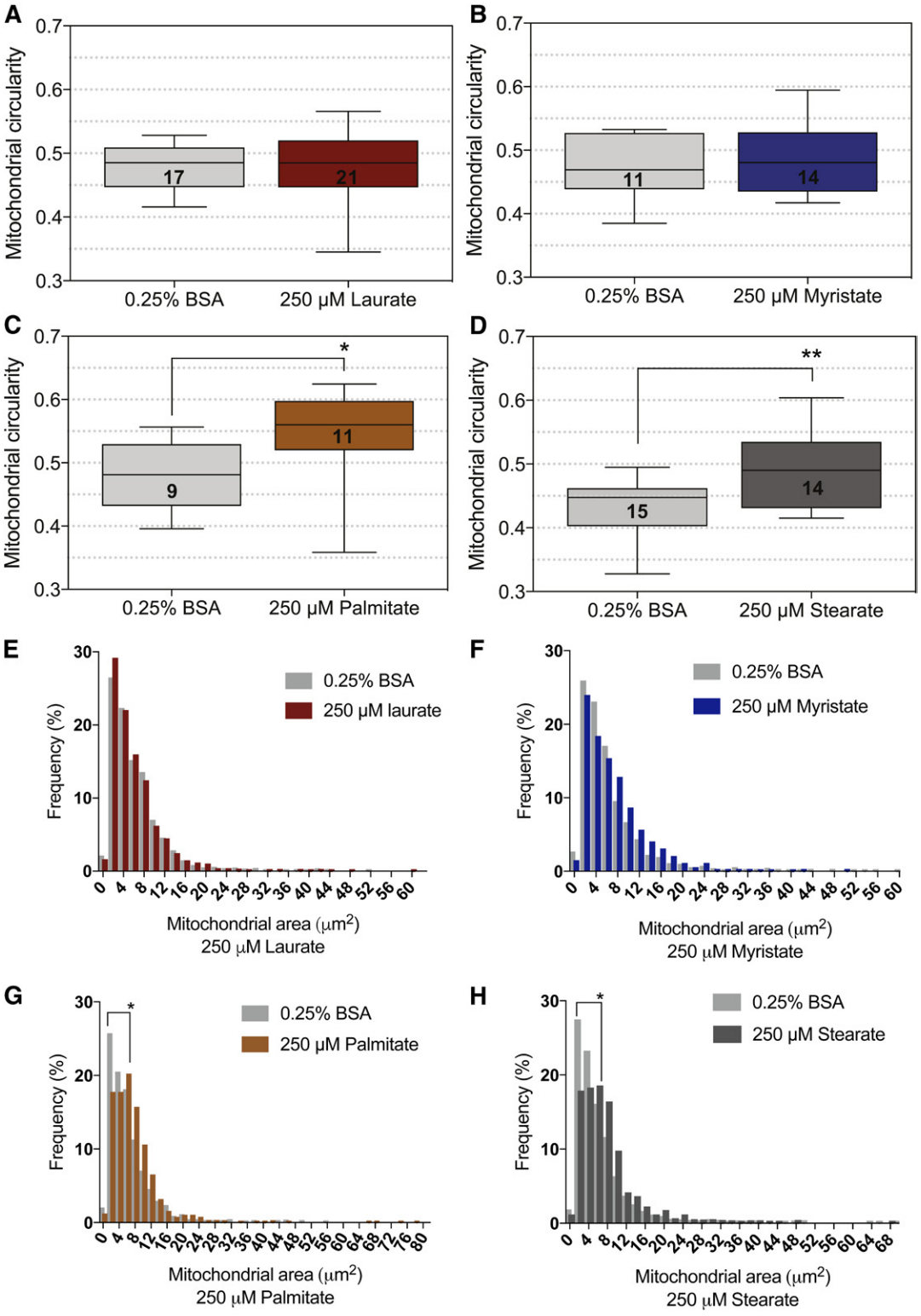

Fig. 6. LCSFAs palmitate and stearate alter mitochondrial morphology in mouse DRG neurons. Mitochondrial circularity was not significantly affected by 250 μM laurate or 250 μM myristate (A, B), but a significant increase in circularity was observed in 250 μM palmitate and 250 μM stearate-treated DRG neurons (C, D). E, F: The distribution of mitochondrial size in DRG neurons treated with 250 μM laurate and myristate matched the mitochondrial size profile of the 0.25% BSA control. G, H: Treatment with 250 μM palmitate or 250 μM stearate induced a shift in the mitochondrial size profile, resulting in larger mitochondria relative to the 0.25% BSA control. The number of DRG neurons analyzed for changes in mitochondrial morphology are listed in the box plot of each condition. Values are expressed as mean ± SEM. * $P < 0.05$, unpaired *t*-test for mitochondrial circularity and Kolmogorov-Smirnov test for mitochondrial size distribution.

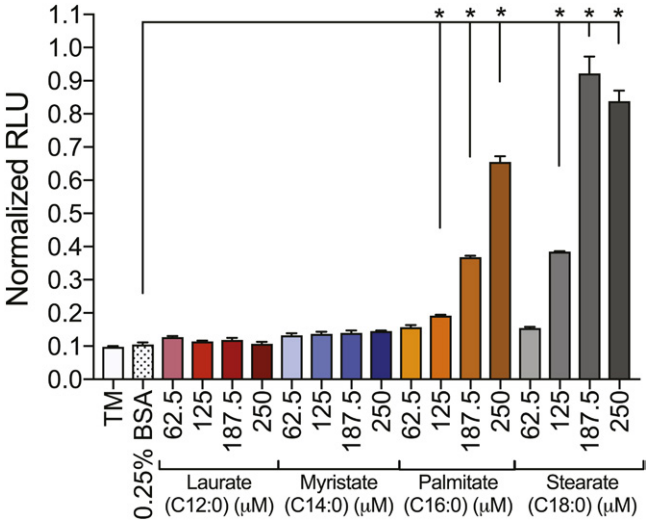

Fig. 7. Caspase 3/7 activity is increased in 50B11 DRG neurons exposed to elevated levels of palmitate and stearate. No significant increases in caspase 3/7 activity resulted from laurate and myristate treatments ranging from 62.5 to 250 μM compared with the TM and 0.25% BSA control. Concentrations of 187.5–250 μM palmitate and stearate led to a dose-dependent amplification of caspase 3/7 activity, whereas 62.5 μM palmitate and stearate maintained basal caspase 3/7 activation levels. Values are expressed as mean ± SEM. * $P < 0.01$, ordinary one-way ANOVA with Tukey's multiple-comparisons test.

cargo encounters stationary organelles in both the retrograde and anterograde directions. Therefore, the increase in stationary mitochondria in DRG axons exposed to LCSFAs likely triggers a significant decrease in velocity of motile mitochondria.

Mitochondrial depolarization corresponds with impairment of mitochondrial trafficking in palmitate- and stearate-treated DRG neurons, again supporting the premise that the percentage of depolarized mitochondria is dependent on SFA hydrocarbon chain length. These results are in line with previous studies that identify a correlation between mitochondrial depolarization and impaired mitochondrial trafficking using inhibitors of the mitochondrial electron transport chain (71, 72). We also showed that LCSFAs palmitate and stearate reduce the level of intracellular ATP in DRG neurons and that the degree to which the ATP level is reduced depends on hydrocarbon chain length. These results are consistent with previous studies that identify LCSFAs as uncouplers of mitochondrial oxidative phosphorylation, whereas MCSFAs promote efficient mitochondrial oxidation (18, 24, 56). Moreover, LCSFAs can open the permeability transition pore, leading to the uncoupling of the mitochondrial membrane (60, 67). This uncoupling potential is higher for LCSFAs than for MCSFAs (18, 67). Because mitochondrial membrane potential is required to drive intracellular ATP synthesis, our results suggest that the high uncoupling potential of LCSFAs palmitate and stearate induce a loss of mitochondrial membrane potential that diminishes ATP production. The ATP deficit in the LCSFA-treated DRG neurons is likely due to uncoupling of oxidative phosphorylation and bioenergetic dyshomeostasis (15, 16). LCSFA-induced mitochondrial depolarization also correlates with alterations in mitochondrial morphology, resulting in larger axonal mitochondria with a higher circularity index (Fig. 6). These morphological changes are a signature of neuronal mitochondrial dysfunction and result from swelling due to a loss of inner membrane structure during the mitochondrial permeability transition pore (73).Together, these results suggest that palmitate- and stearate-induced mitochondrial depolarization may underlie a reduction in ATP synthesis and impairment in mitochondrial trafficking, whereas myristate and laurate have no impact on mitochondrial function and therefore preserve mitochondrial trafficking.

Although SFAs have been previously reported to induce mitochondrial dysfunction and apoptosis in several cell types (50, 51, 74), studies drawing associations between mitochondrial dysfunction and apoptotic effects of MCSFAs and LCSFAs in DRG neurons are limited. We found that palmitate and stearate induced significant increases in caspase 3/7 levels, whereas laurate and myristate had no effect on caspase 3/7 activation. Interestingly, increases in caspase 3/7 activity were only observed at higher concentrations of 187.5–250 μM palmitate and stearate, despite the fact that the 62.5 μM palmitate and stearate treatments impaired mitochondrial trafficking and induced mitochondrial depolarization. These results indicate that mitochondrial depolarization and impaired trafficking likely precede neuronal apoptosis (14, 16, 60). We acknowledge that the concentration of LCSFAs required to enhance apoptosis could be due to inherent metabolic differences in 50B11 cells, a transformed DRG cell line (42), compared with primary DRG neurons; however, the current data support our contention that abnormal mitochondrial trafficking and mitochondrial depolarization correlate with increased DRG neuronal apoptosis. These results are further supported by literature demonstrating that mitochondrial depolarization leads to cytochrome c release and energetic failure, resulting in the activation of apoptosis (41, 75–77).

Overall, our study suggests that the energetically challenging LCSFAs palmitate and stearate impair mitochondrial trafficking and function, thereby leading to DRG neuronal apoptosis. Conversely, the shorter-chain SFAs myristate and laurate have no impact on the function or axonal transport of mitochondria in DRG neurons. Our current data have also defined a distinct SFA hydrocarbon chain length cutoff; SFAs with a length ≤C14:0 maintain complete DRG mitochondrial transport and function, whereas C16:0–C18:0 LCSFAs abolish mitochondrial trafficking, impair mitochondrial function, and activate apoptotic pathways. These studies identify a highly specific metabolic regulation of DRG neuronal mitochondrial function related to the hydrocarbon chain length of SFAs and provide new mechanistic insight into the association of dyslipidemia and DPN.

The authors thank Dr. Stacey Sakowski Jacoby for her expert editorial advice; Dr. Ahmet Hoke (Johns Hopkins University, Baltimore, MD) for the kind gift of 50B11 DRG neurons; and Dr. Sami Barmada for his assistance with the mitochondrial morphology analysis. Confocal microscopy and image analysis were completed at the Michigan Diabetes Research Center's Microscopy and Image Analysis Core, supported by NIDDK Grant P60DK020572.

REFERENCES

1. Callaghan, B. C., R. S. Price, and E. L. Feldman. 2015. Distal symmetric polyneuropathy: a review. *JAMA*. **314:** 2172–2181.
2. Cortez, M., J. R. Singleton, and A. G. Smith. 2014. Glucose intolerance, metabolic syndrome, and neuropathy. *Handb. Clin. Neurol.* **126:** 109–122.
3. Centers for Disease Control and Prevention. 2014. National Diabetes Statistics Report: Estimates of Diabetes and Its Burden in the United States. Department of Health and Human Services, Atlanta.
4. Boulton, A. J., A. I. Vinik, J. C. Arezzo, V. Bril, E. L. Feldman, R. Freeman, R. A. Malik, R. E. Maser, J. M. Sosenko, D. Ziegler, et al. 2005. Diabetic neuropathies: a statement by the American Diabetes Association. *Diabetes Care.* **28:** 956–962.
5. Breton, M. C., L. Guenette, M. A. Amiche, J. F. Kayibanda, J. P. Gregoire, and J. Moisan. 2013. Burden of diabetes on the ability to work: a systematic review. *Diabetes Care.* **36:** 740–749.
6. Callaghan, B. C., H. T. Cheng, C. L. Stables, A. L. Smith, and E. L. Feldman. 2012. Diabetic neuropathy: clinical manifestations and current treatments. *Lancet Neurol.* **11:** 521–534.
7. Edwards, J. L., A. M. Vincent, H. T. Cheng, and E. L. Feldman. 2008. Diabetic neuropathy: mechanisms to management. *Pharmacol. Ther.* **120:** 1–34.
8. Smith, A. G., J. Russell, E. L. Feldman, J. Goldstein, A. Peltier, S. Smith, J. Hamwi, D. Pollari, B. Bixby, J. Howard, et al. 2006. Lifestyle intervention for pre-diabetic neuropathy. *Diabetes Care.* **29:** 1294–1299.
9. Vincent, A. M., L. M. Hinder, R. Pop-Busui, and E. L. Feldman. 2009. Hyperlipidemia: a new therapeutic target for diabetic neuropathy. *J. Peripher. Nerv. Syst.* **14:** 257–267.
10. Hinder, L. M., P. D. O'Brien, J. M. Hayes, C. Backus, A. P. Solway, C. Sims-Robinson, and E. L. Feldman. 2017. Dietary reversal of neuropathy in a murine model of prediabetes and metabolic syndrome. *Dis. Model. Mech.* **10:** 717–725.
11. Boden, G. 1999. Free fatty acids, insulin resistance, and type 2 diabetes mellitus. *Proc. Assoc. Am. Physicians.* **111:** 241–248.
12. Nolan, C. J., and C. Z. Larter. 2009. Lipotoxicity: why do saturated fatty acids cause and monounsaturates protect against it? *J. Gastroenterol. Hepatol.* **24:** 703–706.
13. O'Brien, P. D., L. M. Hinder, S. A. Sakowski, and E. L. Feldman. 2014. ER stress in diabetic peripheral neuropathy: a new therapeutic target. *Antioxid. Redox Signal.* **21:** 621–633.
14. Hinder, L. M., C. Figueroa-Romero, C. Pacut, Y. Hong, A. Vivekanandan-Giri, S. Pennathur, and E. L. Feldman. 2014. Long-chain acyl coenzyme A synthetase 1 overexpression in primary cultured Schwann cells prevents long chain fatty acid-induced oxidative stress and mitochondrial dysfunction. *Antioxid. Redox Signal.* **21:** 588–600.
15. Hinder, L. M., A. M. Vincent, C. F. Burant, S. Pennathur, and E. L. Feldman. 2012. Bioenergetics in diabetic neuropathy: what we need to know. *J. Peripher. Nerv. Syst.* **17(Suppl 2):** 10–14.
16. Rumora, A. E., S. I. Lentz, L. M. Hinder, S. W. Jackson, A. Valesano, G. E. Levinson, and E. L. Feldman. 2018. Dyslipidemia impairs mitochondrial trafficking and function in sensory neurons. *FASEB J.* **32:** 195–207.
17. Feldman, E. L., K. A. Nave, T. S. Jensen, and D. L. H. Bennett. 2017. New horizons in diabetic neuropathy: mechanisms, bioenergetics, and pain. *Neuron.* **93:** 1296–1313.
18. Schönfeld, P., and L. Wojtczak. 2016. Short- and medium-chain fatty acids in energy metabolism: the cellular perspective. *J. Lipid Res.* **57:** 943–954.
19. Papamandjaris, A. A., D. E. MacDougall, and P. J. Jones. 1998. Medium chain fatty acid metabolism and energy expenditure: obesity treatment implications. *Life Sci.* **62:** 1203–1215.
20. Pankow, J. S., B. B. Duncan, M. I. Schmidt, C. M. Ballantyne, D. J. Couper, R. C. Hoogeveen, S. H. Golden, and Atherosclerosis Risk in Communities Study. 2004. Fasting plasma free fatty acids and risk of type 2 diabetes: the Atherosclerosis Risk in Communities Study. *Diabetes Care.* **27:** 77–82.
21. Wang, L., A. R. Folsom, Z. J. Zheng, J. S. Pankow, J. H. Eckfeldt, and ARIC Study Investigators. 2003. Plasma fatty acid composition and incidence of diabetes in middle-aged adults: the Atherosclerosis Risk in Communities (ARIC) Study. *Am. J. Clin. Nutr.* **78:** 91–98.
22. Chen, B., Y. Huang, D. Zheng, R. Ni, and M. A. Bernards. 2018. Dietary fatty acids alter lipid profiles and induce myocardial dysfunction without causing metabolic disorders in mice. *Nutrients.* **10:** E106.
23. International Diabetes Foundation. 2015. IDF Diabetes Atlas, 7th edition. International Diabetes Foundation, Brussels, Belgium.
24. Wein, S., S. Wolffram, J. Schrezenmeir, D. Gasperikova, I. Klimes, and E. Sebokova. 2009. Medium-chain fatty acids ameliorate insulin resistance caused by high-fat diets in rats. *Diabetes Metab. Res. Rev.* **25:** 185–194.
25. Wang, M. E., B. K. Singh, M. C. Hsu, C. Huang, P. M. Yen, L. S. Wu, D. S. Jong, and C. H. Chiu. 2017. Increasing dietary medium-chain fatty acid ratio mitigates high-fat diet-induced non-alcoholic steatohepatitis by regulating autophagy. *Sci. Rep.* **7:** 13999.
26. Montgomery, M. K., B. Osborne, S. H. Brown, L. Small, T. W. Mitchell, G. J. Cooney, and N. Turner. 2013. Contrasting metabolic effects of medium- versus long-chain fatty acids in skeletal muscle. *J. Lipid Res.* **54:** 3322–3333.
27. Egnatchik, R. A., A. K. Leamy, Y. Noguchi, M. Shiota, and J. D. Young. 2014. Palmitate-induced activation of mitochondrial metabolism promotes oxidative stress and apoptosis in H4IIEC3 rat hepatocytes. *Metabolism.* **63:** 283–295.
28. Sheng, Z. H. 2014. Mitochondrial trafficking and anchoring in neurons: new insight and implications. *J. Cell Biol.* **204:** 1087–1098.
29. Cai, Q., M. L. Davis, and Z. H. Sheng. 2011. Regulation of axonal mitochondrial transport and its impact on synaptic transmission. *Neurosci. Res.* **70:** 9–15.
30. Pekkurnaz, G., J. C. Trinidad, X. Wang, D. Kong, and T. L. Schwarz. 2014. Glucose regulates mitochondrial motility via Milton modification by O-GlcNAc transferase. *Cell.* **158:** 54–68.
31. Schwarz, T. L. 2013. Mitochondrial trafficking in neurons. *Cold Spring Harb. Perspect. Biol.* **5:** a011304.
32. Macaskill, A. F., J. E. Rinholm, A. E. Twelvetrees, I. L. Arancibia-Carcamo, J. Muir, A. Fransson, P. Aspenstrom, D. Attwell, and J. T. Kittler. 2009. Miro1 is a calcium sensor for glutamate receptor-dependent localization of mitochondria at synapses. *Neuron.* **61:** 541–555.
33. Misgeld, T., and T. L. Schwarz. 2017. Mitostasis in neurons: maintaining mitochondria in an extended cellular architecture. *Neuron.* **96:** 651–666.
34. Vincent, A. M., J. M. Hayes, L. L. McLean, A. Vivekanandan-Giri, S. Pennathur, and E. L. Feldman. 2009. Dyslipidemia-induced neuropathy in mice: the role of oxLDL/LOX-1. *Diabetes.* **58:** 2376–2385.
35. Vincent, A. M., K. Kato, L. L. McLean, M. E. Soules, and E. L. Feldman. 2009. Sensory neurons and Schwann cells respond to oxidative stress by increasing antioxidant defense mechanisms. *Antioxid. Redox Signal.* **11:** 425–438.
36. Vincent, A. M., J. W. Russell, K. A. Sullivan, C. Backus, J. M. Hayes, L. L. McLean, and E. L. Feldman. 2007. SOD2 protects neurons from injury in cell culture and animal models of diabetic neuropathy. *Exp. Neurol.* **208:** 216–227.
37. De Vos, K. J., A. L. Chapman, M. E. Tennant, C. Manser, E. L. Tudor, K. F. Lau, J. Brownlees, S. Ackerley, P. J. Shaw, D. M. McLoughlin, et al. 2007. Familial amyotrophic lateral sclerosis-linked SOD1 mutants perturb fast axonal transport to reduce axonal mitochondria content. *Hum. Mol. Genet.* **16:** 2720–2728.
38. De Vos, K. J., J. Sable, K. E. Miller, and M. P. Sheetz. 2003. Expression of phosphatidylinositol (4,5) bisphosphate-specific pleckstrin homology domains alters direction but not the level of axonal transport of mitochondria. *Mol. Biol. Cell.* **14:** 3636–3649.
39. De Vos, K. J., and M. P. Sheetz. 2007. Visualization and quantification of mitochondrial dynamics in living animal cells. *Methods Cell Biol.* **80:** 627–682.
40. Nguyen, L. H., D. A. Robinton, M. T. Seligson, L. Wu, L. Li, D. Rakheja, S. A. Comerford, S. Ramezani, X. Sun, M. S. Parikh, et al. 2014. Lin28b is sufficient to drive liver cancer and necessary for its maintenance in murine models. *Cancer Cell.* **26:** 248–261.
41. Russell, J. W., D. Golovoy, A. M. Vincent, P. Mahendru, J. A. Olzmann, A. Mentzer, and E. L. Feldman. 2002. High glucose-induced oxidative stress and mitochondrial dysfunction in neurons. *FASEB J.* **16:** 1738–1748.
42. Chen, W., R. Mi, N. Haughey, M. Oz, and A. Hoke. 2007. Immortalization and characterization of a nociceptive dorsal root ganglion sensory neuronal line. *J. Peripher. Nerv. Syst.* **12:** 121–130.
43. Tank, E. M., C. Figueroa-Romero, L. M. Hinder, K. Bedi, H. C. Archbold, X. Li, K. Weskamp, N. Safren, X. Paez-Colasante, C. Pacut, et al. 2018. Abnormal RNA stability in amyotrophic lateral sclerosis. *Nat. Commun.* **9:** 2845.
44. Merrill, R. A., K. H. Flippo, and S. Strack. 2017. Measuring mitochondrial shape with ImageJ. *In* Techniques to Investigate Mitochondrial Function in Neurons. S. Strack and Y. M. Usachev, editors. Springer Protocols, Vol. 123. Springer, New York. 31–48.

45. Kiryu-Seo, S., N. Ohno, G. J. Kidd, H. Komuro, and B. D. Trapp. 2010. Demyelination increases axonal stationary mitochondrial size and the speed of axonal mitochondrial transport. *J. Neurosci.* **30:** 6658–6666.
46. Lancaster, E., J. Li, T. Hanania, R. Liem, M. A. Scheideler, and S. S. Scherer. 2018. Myelinated axons fail to develop properly in a genetically authentic mouse model of Charcot-Marie-Tooth disease type 2E. *Exp. Neurol.* **308:** 13–25.
47. Che, D. L., P. D. Chowdary, and B. Cui. 2016. A close look at axonal transport: cargos slow down when crossing stationary organelles. *Neurosci. Lett.* **610:** 110–116.
48. Stephen, T. L., N. F. Higgs, D. F. Sheehan, S. Al Awabdh, G. Lopez-Domenech, I. L. Arancibia-Carcamo, and J. T. Kittler. 2015. Miro1 regulates activity-driven positioning of mitochondria within astrocytic processes apposed to synapses to regulate intracellular calcium signaling. *J. Neurosci.* **35:** 15996–16011.
49. Russell, J. W., C. Gong, A. Vincent, A. R. Berent, L. E. Mentzer, and M. Brownlee. 2001. Nitric oxide (NO) and mitochondrial manganese superoxide dismutase (MnSOD) regulate glucose-induced oxidative stress and programmed cell death in neurons. *Neurology.* **56(Suppl 3):** A394.
50. Listenberger, L. L., D. S. Ory, and J. E. Schaffer. 2001. Palmitate-induced apoptosis can occur through a ceramide-independent pathway. *J. Biol. Chem.* **276:** 14890–14895.
51. Savary, S., D. Trompier, P. Andreoletti, F. Le Borgne, J. Demarquoy, and G. Lizard. 2012. Fatty acids—induced lipotoxicity and inflammation. *Curr. Drug Metab.* **13:** 1358–1370.
52. Giles, C., R. Takechi, N. A. Mellett, P. J. Meikle, S. Dhaliwal, and J. C. Mamo. 2016. The effects of long-term saturated fat enriched diets on the brain lipidome. *PLoS One.* **11:** e0166964.
53. Kalmijn, S., L. J. Launer, A. Ott, J. C. Witteman, A. Hofman, and M. M. Breteler. 1997. Dietary fat intake and the risk of incident dementia in the Rotterdam Study. *Ann. Neurol.* **42:** 776–782.
54. Kanoski, S. E., and T. L. Davidson. 2011. Western diet consumption and cognitive impairment: links to hippocampal dysfunction and obesity. *Physiol. Behav.* **103:** 59–68.
55. Lai, M., P. C. Chandrasekera, and N. D. Barnard. 2014. You are what you eat, or are you? The challenges of translating high-fat-fed rodents to human obesity and diabetes. *Nutr. Diabetes.* **4:** e135.
56. Airhart, S., W. T. Cade, H. Jiang, A. R. Coggan, S. B. Racette, K. Korenblat, C. A. Spearie, S. Waller, R. O'Connor, A. Bashir, et al. 2016. A diet rich in medium-chain fatty acids improves systolic function and alters the lipidomic profile in patients with type 2 diabetes: a pilot study. *J. Clin. Endocrinol. Metab.* **101:** 504–512.
57. Nagao, K., and T. Yanagita. 2010. Medium-chain fatty acids: functional lipids for the prevention and treatment of the metabolic syndrome. *Pharmacol. Res.* **61:** 208–212.
58. O'Brien, P. D., S. A. Sakowski, and E. L. Feldman. 2014. Mouse models of diabetic neuropathy. *ILAR J.* **54:** 259–272.
59. Hinder, L. M., A. Vivekanandan-Giri, L. L. McLean, S. Pennathur, and E. L. Feldman. 2013. Decreased glycolytic and tricarboxylic acid cycle intermediates coincide with peripheral nervous system oxidative stress in a murine model of type 2 diabetes. *J. Endocrinol.* **216:** 1–11.
60. Nisr, R. B., and C. Affourtit. 2016. Palmitate-induced changes in energy demand cause reallocation of ATP supply in rat and human skeletal muscle cells. *Biochim. Biophys. Acta.* **1857:** 1403–1411.
61. Eckel, R. H., A. S. Hanson, A. Y. Chen, J. N. Berman, T. J. Yost, and E. P. Brass. 1992. Dietary substitution of medium-chain triglycerides improves insulin-mediated glucose metabolism in NIDDM subjects. *Diabetes.* **41:** 641–647.
62. Ronis, M. J., J. N. Baumgardner, N. Sharma, J. Vantrease, M. Ferguson, Y. Tong, X. Wu, M. A. Cleves, and T. M. Badger. 2013. Medium chain triglycerides dose-dependently prevent liver pathology in a rat model of non-alcoholic fatty liver disease. *Exp. Biol. Med. (Maywood).* **238:** 151–162.
63. Page, K. A., A. Williamson, N. Yu, E. C. McNay, J. Dzuira, R. J. McCrimmon, and R. S. Sherwin. 2009. Medium-chain fatty acids improve cognitive function in intensively treated type 1 diabetic patients and support in vitro synaptic transmission during acute hypoglycemia. *Diabetes.* **58:** 1237–1244.
64. Cai, Q., and Z. H. Sheng. 2009. Moving or stopping mitochondria: Miro as a traffic cop by sensing calcium. *Neuron.* **61:** 493–496.
65. Niescier, R. F., S. K. Kwak, S. H. Joo, K. T. Chang, and K. T. Min. 2016. Dynamics of mitochondrial transport in axons. *Front. Cell. Neurosci.* **10:** 123.
66. Sheng, Z. H. 2017. The interplay of axonal energy homeostasis and mitochondrial trafficking and anchoring. *Trends Cell Biol.* **27:** 403–416.
67. Penzo, D., C. Tagliapietra, R. Colonna, V. Petronilli, and P. Bernardi. 2002. Effects of fatty acids on mitochondria: implications for cell death. *Biochim. Biophys. Acta.* **1555:** 160–165.
68. Saxton, W. M., and P. J. Hollenbeck. 2012. The axonal transport of mitochondria. *J. Cell Sci.* **125:** 2095–2104.
69. Hollenbeck, P. J., and W. M. Saxton. 2005. The axonal transport of mitochondria. *J. Cell Sci.* **118:** 5411–5419.
70. Overly, C. C., H. I. Rieff, and P. J. Hollenbeck. 1996. Organelle motility and metabolism in axons vs dendrites of cultured hippocampal neurons. *J. Cell Sci.* **109:** 971–980.
71. Miller, K. E., and M. P. Sheetz. 2004. Axonal mitochondrial transport and potential are correlated. *J. Cell Sci.* **117:** 2791–2804.
72. Cai, Q., H. M. Zakaria, A. Simone, and Z. H. Sheng. 2012. Spatial parkin translocation and degradation of damaged mitochondria via mitophagy in live cortical neurons. *Curr. Biol.* **22:** 545–552.
73. Rintoul, G. L., and I. J. Reynolds. 2010. Mitochondrial trafficking and morphology in neuronal injury. *Biochim. Biophys. Acta.* **1802:** 143–150.
74. Kitaura, Y., K. Inoue, N. Kato, N. Matsushita, and Y. Shimomura. 2015. Enhanced oleate uptake and lipotoxicity associated with laurate. *FEBS Open Bio.* **5:** 485–491.
75. Lemasters, J. J., A. L. Nieminen, T. Qian, L. C. Trost, S. P. Elmore, Y. Nishimura, R. A. Crowe, W. E. Cascio, C. A. Bradham, D. A. Brenner, et al. 1998. The mitochondrial permeability transition in cell death: a common mechanism in necrosis, apoptosis and autophagy. *Biochim. Biophys. Acta.* **1366:** 177–196.
76. Heiskanen, K. M., M. B. Bhat, H. W. Wang, J. Ma, and A. L. Nieminen. 1999. Mitochondrial depolarization accompanies cytochrome c release during apoptosis in PC6 cells. *J. Biol. Chem.* **274:** 5654–5658.
77. Kadenbach, B., S. Arnold, I. Lee, and M. Huttemann. 2004. The possible role of cytochrome c oxidase in stress-induced apoptosis and degenerative diseases. *Biochim. Biophys. Acta.* **1655:** 400–408.